2 Laser Medicine and Medical Imaging

Sponsors

National Institutes of Health
Contract NIH-RO1-CA75289-03
Contract NIH-RO1-EY11289-13
Contract NIH-RO1-AR44812-02
Contract NIH-R29-HL55686-01A1
U.S. Air Force – Office of Scientific Research
Contract F49620-98-1-0139
U.S. Navy – Office of Naval Research/MFEL
Contract N000014-97-1-1066
Whittaker Foundation
Contract 96-0205

Project Staff

Stephen A. Boppart, Ravi K. Ghanta, Pei-Lin Hsiung, Tony Ko, Christine A. Jesser, Constantinos Pitris, Kathleen Saunders, Dr. Mark E. Brezinski, Dr. Christian Chudoba, Dr. Wolfgang Drexler, Dr. Ingmar Hartl, Dr. Xingde Li, Dr. Uwe Morgner, Dr. Joel Schuman, Dr. Debra L. Stamper, Professor James G. Fujimoto

2.1 Optical Coherence Tomography Technology

Ultrahigh Resolution Optical Coherence Tomography

Optical coherence tomography (OCT) is an emerging diagnostic technology, developed by our research group and collaborators in 1991,[28] that is being investigated for applications in a number of medical fields. OCT can produce high resolution cross sectional images of internal microstructure. OCT imaging is somewhat analogous to ultrasound imaging except that light is used instead of sound. Because the velocity of light is much higher than that of sound, OCT imaging is based on low coherence interferometry. Low-coherence light is sent into a Michelson interferometer consisting of two arms, a sample arm and a reference arm. The backscattered light from the sample is measured, and its position is located by varying the optical path length in the reference arm. An interferometric signal is generated only when the phase delay of the light collected from the sample arm matches the phase delay in the reference arm to within the coherence length of the source. A two-dimensional OCT image is built up with a series of these adjacent axial scans.

The axial resolution of OCT (typically 10-15 μm) is mainly limited by the bandwidth of the low-coherence light source, usually a superluminescent diode. This resolution provides more detailed structural information of architectural tissue morphology than any other conventional technique, but is insufficient to identify individual cells or to assess subcellular structures such as nuclei or mitotic figures. The first sub-10-μm-resolution was achieved by using broadband fluorescence from organic dye[29] and from Ti:sapphire[30] lasers, but due to their low brightness, biological im-

[28] D. Huang, E. Swanson, C.P. Lin, J.S. Schuman, W.G. Stinson, W. Chang, M.R. Hee, T. Flotte, K. Gregory, C.A. Puliafito, and J.G. Fujimoto, "Optical Coherence Tomography," *Science* 254: 1178-81 (1991).

[29] H.H. Liu, P.H. Cheng, and J. Wang, "Spatially Coherent White Light Interferometer Based on a Point Flourescent Source," *Opt. Lett*. 18: 678-80 (1993).

[30] X. Clivaz, F. Marquis-Weible, and R.P.Salathe, "Optical Low Coherence Teflectometry with 1.9 μm Spatial Resolution," *Elec. Lett*. 28: 1553-55 (1992).

aging could not be performed. Recent developments in femtosecond Kerr-lens mode locking of solid-state lasers have enabled the generation of low-coherence light for OCT with a single transverse mode and powers of more than 100 mW.[31,32] High image resolutions of 5 μm with 2-3 mm imaging penetration depths in scattering tissue using a Cr^{4+}:forsterite laser emitting light at 1300 nm has permitted microscopic visualization of dynamic morphological and functional changes that occur during embryonic development.[33]

Although previous studies have demonstrated *in vivo* cellular OCT imaging of tissue morphology, most have imaged tissue at ~5-10 μm resolution. Our group has recently developed and demonstrated an ultrahigh resolution OCT system using a state-of-the-art, ultrabroad bandwidth, Kerr-lens modelocked Ti:Al_2O_3 laser.[34] This laser source produces pulse durations of only two-cycles with bandwidths of up to 350 nm centered at 800 nm. By carefully matching dispersion (especially higher orders), minimizing chromatic aberrations, and optimizing optics, fibers, electronics, and data acquisition, a fiber-optic OCT system has been developed (Figure 9). *In vivo* subcellular imaging with longitudinal resolutions of 1 μm and transverse resolutions of 3 μm has been achieved. To our knowledge, this represents the highest axial resolution demonstrated for *in vivo* OCT imaging.[35]

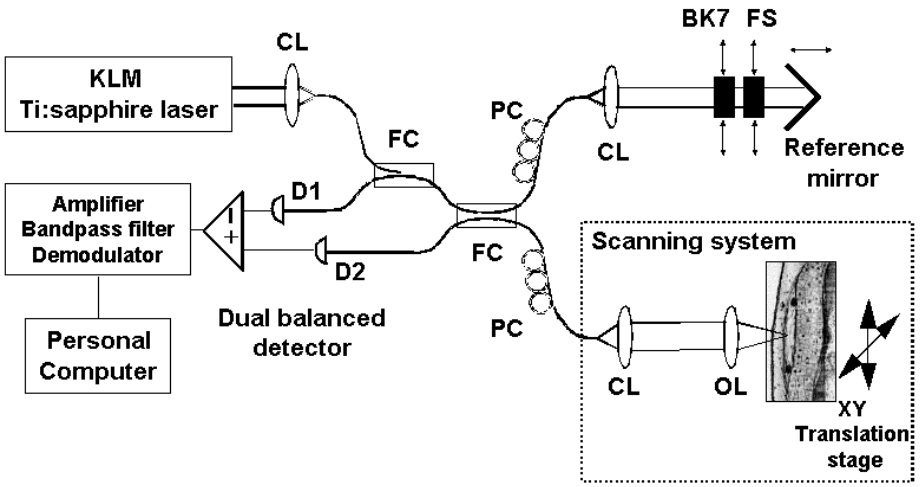

Figure 9: Ultrahigh-resolution OCT schematic. Abbreviations: BK7, glass prism; CL, collimating lens; D1, D2, detectors; FC, fiber coupler; FS, glass prism; OL, objective lens; PC, polarization controller.

---

[31] B.E Bouma, G.J. Tearney, I.P. Bilinsky, B. Golubovic, and J.G. Fujimoto, "A Self-Phase-Modulated Kerr-Lens-Modelocked Cr:forsterite Laser Source for Optical Coherence Tomography," *Opt. Lett.* 21: 1839-41 (1996).

[32] B.E Bouma, G.J. Tearney, S.A. Boppart, M.R. Hee, M.E. Brezinski, and J.G. Fujimoto, "High Resolution Optical Coherence Tomographic Imaging using a Modelocked Ti:Al_20_3 Laser," *Opt. Lett*. 20: 1486-88 (1995).

[33] S.A. Boppart, B.E. Bouma, C. Pitris, J.F. Southern, M.E. Brezinski, and J.G. Fujimoto, "*In Vivo* Cellular Optical Coherence Tomography Imaging," *Nature Med*. 4: 861-64 (1998).

[34] U. Morgner, F.X. Kärtner, S.H. Cho, Y. Chen, H.A. Haus, J.G. Fujimoto, E.P. Ippen, V. Scheuer, G. Angelow, and T. Tschudi, "Sub-Two-Cycle Pulses from a Kerr-Lens Mode-Locked Ti:sapphire Laser," *Opt. Lett*. 24: 411-13 (1999).

[35] W. Drexler, U. Morgner, F.X. Kärtner, C. Pitris, S.A. Boppart, X.D. Li, E.P. Ippen, and J.G. Fujimoto, "*In Vivo* Ultrahigh Resolution Optical Coherence Tomography," *Opt. Lett*. 24: 1221-23 (1999).

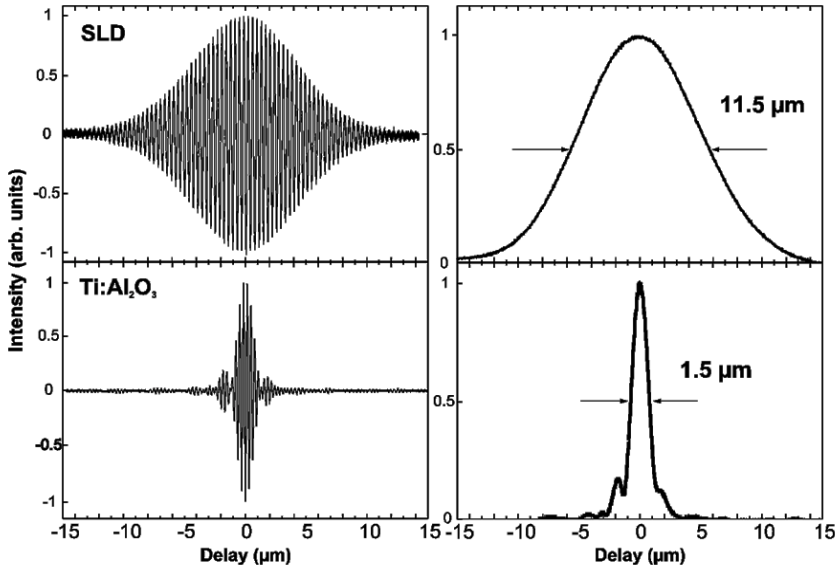

Figure 10: Interference fringe and coherence envelope comparison between the ultrahigh resolution OCT source ($Ti:Al_2O_3$) and a superluminescent diode (SLD). The full-width half-maximum of the envelope (right column) represents the axial resolution in free space.

Since scattering is the predominant mechanism of attenuation at near-infrared wavelengths (800 nm), the imaging depth in non-transparent tissue is limited to 0.5 to 1.0 mm.[36] This depth is less for imaging with wavelengths in the 1300 nm region, but is sufficient to image superficial layers of biological tissues. In addition, the spectral region at 800 nm is important because it overlaps absorption features of several important biological chromophores, e.g. melanin, oxy- and deoxyhemoglobin, and may enable the functional imaging of hemoglobin oxygen saturation. Figure 10 shows a comparison of the coherence lengths (axial resolution) between a superluminescent diode (SLD) and the Ti:sapphire laser ($Ti:Al_2O_3$).

Cellular Morphology

Ultrahigh-resolution OCT is capable of *in vivo* subcellular imaging, which may ultimately have a role in the early diagnosis of human malignancies. Developmental and cellular biology are research fields that have burgeoned within recent years due to advances in molecular biology techniques. OCT can produce high resolution cross-sectional images of biological tissue *in vivo* and in real time.[28,37-39] OCT has been demonstrated for high resolution *in vivo* imaging of developmental processes, including morphological abnormalities and functional parameters.[33,40-

[36] J.M. Schmitt, A. Knuttel, M. Yadlowsky, and A.A. Eckhaus, "Optical Coherence Tomography of a Dense Tissue: Statistics of Attenuation and Backscattering," *Phys. Med. Biol*. 39: 1705-20 (1994).

[37] J.M. Schmitt, M.J. Yadlowsky, and R.F. Bonner, "Subsurface Imaging of Living Skin with Optical Coherence Microscopy," *Dermatology* 191: 93-98 (1995).

[38] M.E. Brezinski, G.J. Tearney, B.E. Bouma, J.A. Izatt, M.R. Hee, E.A. Swanson, J.F. Southern, and J.G. Fujimoto, "Optical Coherence Tomography for Optical Biopsy: Properties and Demonstration of Vascular Pathology," *Circulation* 93: 1206-13 (1996).

[39] J.G. Fujimoto, M.E. Brezinski, G.J. Tearney, S.A. Boppart, B.E. Bouma, M.R. Hee, J.F. Southern, and E.A. Swanson, "Biomedical iImaging and Optical Biopsy using Optical Coherence Tomography," *Nature Medicin*e 1: 970-72 (1995).

[40] S.A. Boppart, M.E. Brezinski, B.E. Bouma, G.J. Tearney, and J.G. Fujimoto, "Investigation of Developing Embryonic Morphology using Optical Coherence Tomography," *Dev. Biol*. 177: 54-63 (1996).

[43] With the advent of molecular biology and genetic techniques that can site-specifically modify the genome of animal models, OCT has been shown to be a useful tool to image and trace the morphologic and functional expression of the genetic code.

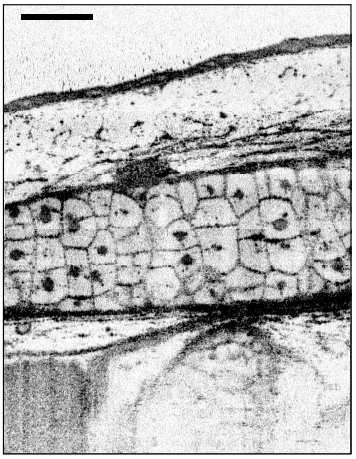

Figure 11: *In vivo* subcellular imaging of *Xenopus* laevis (African frog) tadpole mesenchymal cells at ultrahigh resolutions. Arrows indicate cells which have recently divided. Abbreviations: OT, olfactory tract.

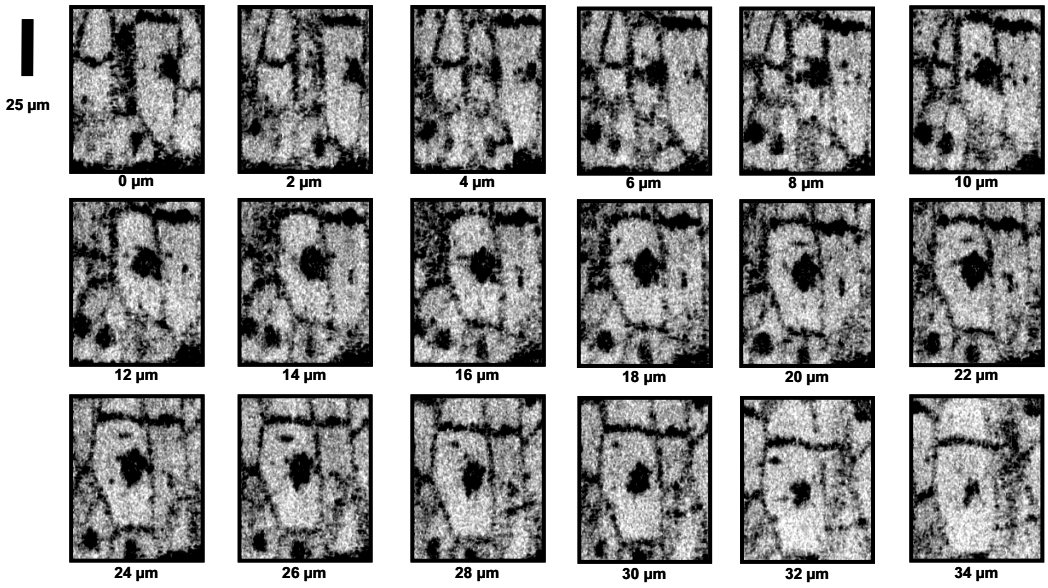

Figure 12: Eighteen *in vivo* tomograms spaced 2 µm apart comprising a 3-D volume of a *Xenopus* mesenchymal cell.

---

[41] S.A. Boppart, M.E. Brezinski, G.J. Tearney, B.E. Bouma, and J.G. Fujimoto, "Imaging Developing Neural Morphology using Optical Coherence Tomography," *J. Neurosci. Meth*. 70: 65-72 (1996).

[42] S.A. Boppart, G.J. Tearney, B.E. Bouma, J.F. Southern, M.E. Brezinski, and J.G. Fujimoto, "Noninvasive Assessment of the Developing *Xenopus* Cardiovascular System using Optical Coherence Tomography," *Proc. Natl. Acad. Sci. USA* 94: 4256-61 (1997).

[43] S. Yazdanfar, M.D. Kulkarni, and J.A. Izatt, "High Resolution Imaging of *In Vivo* Cardiac Dynamics using Color Doppler Optical Coherence Tomography," *Opt. Express* 1: 424-31 (1997).

Figures 11 and 12 demonstrate the feasibility of this novel system for *in vivo* subcellular imaging of a *Xenopus laevis* (African frog tadpole). An area of 0.75 x 0.5 mm (1700 x 1000 pixels) has been imaged and is shown in Figure 11. A three-dimensional sequence consisting of eighteen tomograms spaced 2 μm apart and covering approximately half of a *Xenopus laevis* cell is depicted in Figure 12. Each tomogram represents an area of 70 x 50 μm and consists of 170 x 100 pixels with 0.4 x 0.5 μm pixel spacing. A resolution of 1 x 3 μm (longitudinal x transverse) could be achieved in both figures. Cell membranes and cell nuclei of pleomorphic mesenchymal cells in different stages of mitosis (see two cells indicated by arrows in Figure 11), in addition to tissue morphology like the neural olfactory tract (OT), can be visualized. To overcome depth-of-field limitations and maintain high transverse resolution at varying depths through the image, a zone-focus and image-fusion technique was used. Multiple tomograms were recorded with the focus set to different depths within the specimen, each being in focus over a depth range comparable to the confocal parameter of approximately 40 μm. The in-focus regions from each image were then fused into a single tomogram with greatly extended depth-of-field. This technique is similar to C-mode scanning used in high-frequency ultrasound imaging and has been used for the first time for OCT imaging. In Figure 12, the back surface of the cell (at 0 μm), cell membranes and nuclei, as well as intracellular morphology (especially at 20 μm to 26 μm), can be clearly visualized.

Ultrahigh Resolution Ophthalmic Imaging

OCT has perhaps been most widely investigated in ophthalmology, where it is beginning to make a clinical impact in the assessment of retinal diseases such as macular holes, age-related macular degeneration, glaucoma, and diabetic retinopathy.[28,44-46] Current clinical practice calls for the development of techniques to diagnose ophthalmic disease in its early stages, when treatment is most effective and significant irreversible damage can either be prevented or delayed. With typical axial resolutions of 10 μm, OCT already provides more detailed structural information than any other conventional imaging technique. However the detection of many of the early changes associated with diseases can require more accurate quantification of retinal structure than is possible with standard resolution OCT.

Using the broad bandwidth of our ultrahigh resolution OCT system, we can image with axial resolutions greater than 3 μm (in the retina), corresponding to a factor of 5 improvement over OCT technology using superluminescent diode sources. The signal to noise ratio for the system is ~100 dB. This system enables a significant improvement in the visualization of intraretinal structures for earlier diagnosis and more precise staging of pathology (Figure 13). To our knowledge, the image shown in Figure 13 represents the highest resolution *in vivo* image ever acquired of the human retina. Ultrahigh resolution OCT offers an unprecedented visualization of retinal morphology with structures such as the retinal nerve fiber layer, retinal pigment epithelium, and the inner and outer plexiform layers. These structures are relevant in a variety of retinal diseases, including age-related macular degeneration, diabetic retinopathy, and glaucoma (the three leading causes of blindness worldwide).

---

[44] M.R. Hee, C.A. Puliafito, J.S. Duker, E. Reichel, J.G. Coker, J.R. Wilkins, J.S. Schuman, E.A Swanson, and J.G. Fujimoto, "Topography of Diabetic Macular Edema with Cptical Coherence Tomography," *Ophthalmology* 105: 360-70 (1998).

[45] C.A. Puliafito, M.R. Hee, C.P. Lin, E. Reichel, J.S. Schuman, J.S. Duker, J.A. Izatt, E.A. Swanson, and J.G. Fujimoto, "Imaging of Macular Disease with Optical Coherence Tomography (OCT)," *Ophthalmology* 192: 217-29 (1995).

[46] J.S. Schuman, T. Pedut-Kloizman, E. Hertzmark, M.R. Hee, J.R. Wilkins, J.G. Coker, C.A. Puliafito, J.G. Fujimoto, and E.A. Swanson, "Reproducibility of Nerve Fiber Layer Thickness Measurements using Optical Coherence Tomography," *Ophthalmology* 103: 1889-98 (1996)

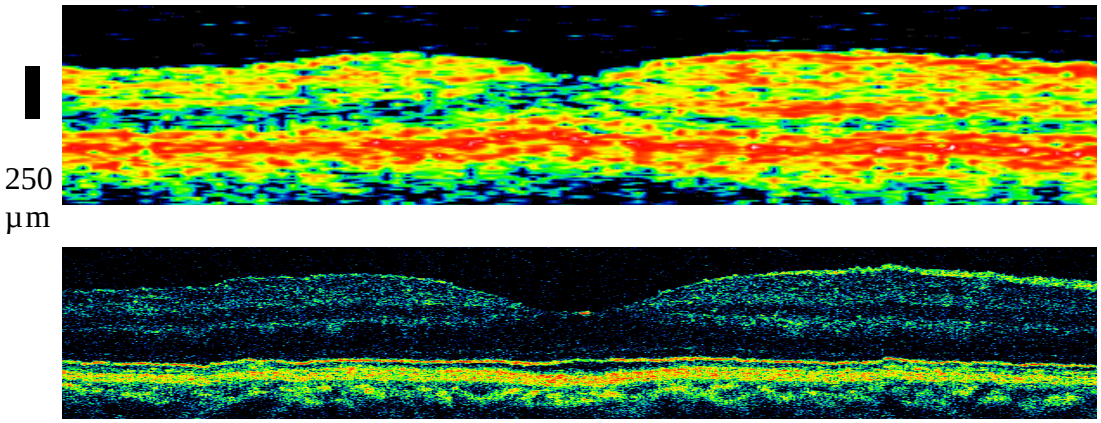

Figure 13: *In Vivo* standard resolution (top) and ultrahigh resolution (bottom) OCT images of a normal human fovea at approximately the same site. Resolutions were 10-15 µm (axial) x 15 µm (transverse) and 3 µm (axial) x 15 µm (transverse) respectively. The standard resolution image was acquired over a 3.59 mm (axial) x 6.00 mm (transverse) region and consists of 500 (axial) x 100 (transverse) pixels. The ultrahigh resolution image was acquired over a 1.50 mm (axial) x 6.00 mm (transverse) region and consists of 1000 (axial) x 600 (transverse) pixels.

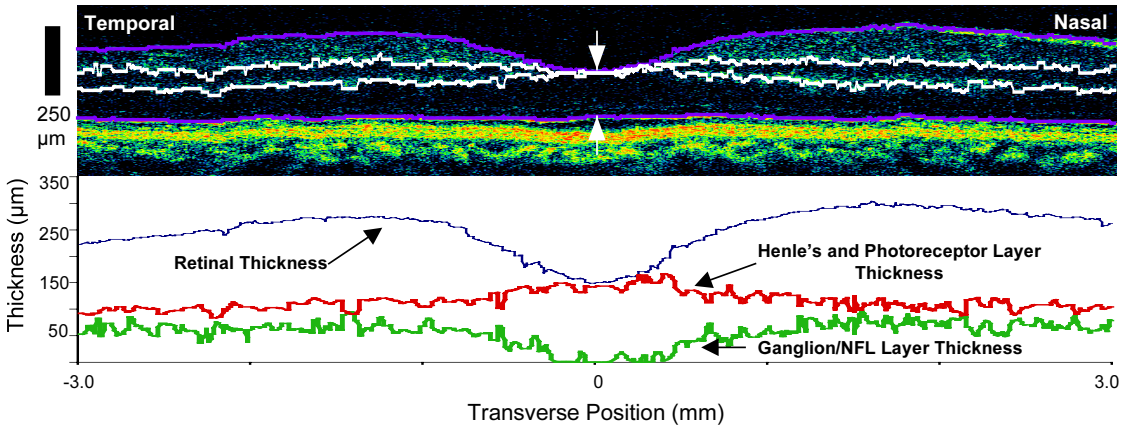

Figure 14: Ultrahigh resolution allows for an unprecedented visualization of intraretinal structures, which may also be quantified to provide an objective measure of retinal disease. The ultrahigh resolution OCT tomogram shown in Figure 13 was segmented and the retina was identified (delineated by purple lines, top). The measured retinal thickness is shown in the graph. The retina was then further segmented into 3 intraretinal layers. The topmost layer consists of the ganglion cell bodies and the retinal nerve fiber layer. The thickness of this layer is shown in the graph. The middle layer consists of the inner nuclear layer and inner plexiform layers. The bottom layer consists of the photoreceptors and Henle's layer. The thickness of this layer is shown in the graph.

Image processing techniques can be applied to acquired tomograms to quantify retinal and intraretinal structures relevant to disease. Figure 14 illustrates the application of preliminary image processing segmentation algorithms to ultrahigh resolution OCT images to quantify retinal and intraretinal structures. Ultrahigh resolution enables the quantification of layers relevant to retinal disease, which were previously not visualized or quantified using standard resolution OCT. Precise quantification of the retinal thickness is important for the diagnosis and staging of macular edema and diabetic retinopathy. Quantification of the photoreceptor and Henle's layer may be

important in a variety of retinal diseases. Quantification of the ganglion cell layer and the nerve fiber layer is important in retinal diseases such as glaucoma.

The visualization and quantification of retinal and intraretinal layers should serve as a valuable clinical tool for the early assessment of ophthalmic disease. Future work will involve ultrahigh resolution OCT imaging studies of patients with retinal diseases such as age-related macular degeneration, diabetic retinopathy, and glaucoma.

Spectroscopic OCT Imaging

In standard OCT imaging only the envelope of the interference signal is detected. Spectral information of the investigated tissue can be obtained by measuring the full interference signal and using digital signal post processing, for example, the Morlet-Wavelet transform or the short-time Fourier transform.[47] This extension of OCT is closely related to classical Fourier transform infrared spectroscopy and has the advantage that the spectroscopic information can be acquired at multiple wavelengths across the available bandwidth of the light source in a single measurement. The ultrahigh-resolution OCT system[35] described previously provides a broad optical spectrum between 650 nm and 1000 nm. This spectral region is of interest to biomedical investigators because it overlaps specific absorption wavelengths for oxy- and deoxyhemoglobin and may enable functional imaging of hemoglobin oxygen saturation. The additional information content from the backscattered signal can be used to enhance image contrast by indicating structures that are more or less scattering at particular wavelengths of light. This "spectroscopic staining" is somewhat analogous to histological staining in standard light microscopy of histopathology.

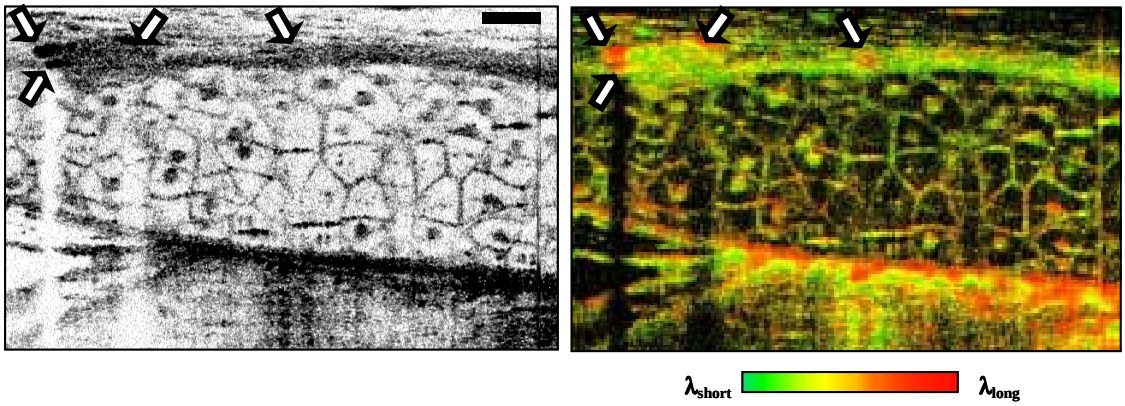

Figure 15: Conventional amplitude (left) and spectroscopic (right) *in vivo* OCT tomograms of *Xenopus* mesenchymal cells. Color scale indicates spectral scattering of light from within tissue. Arrows indicate highly scattering melanocytes. Bar represents 50 μm.

As a first approach, the "center of mass" of the spectra was calculated and represented in a multidimensional map. Hue, saturation, luminance (HSL) color space (not RBG) were used to map the backscattering intensity into the saturation and the spectral center of mass into the hue, keeping luminance constant.[47] This permits the intensity and spectral shift of the backscattered light to be visualized. Figure 15 shows a conventional ultrahigh-resolution OCT image (left) and a spectroscopic OCT image (right) of the same site in a *Xenopus laevis* tadpole *in vivo*. Red hue indicates a long wavelength enhancement of the backscattered light, while green hue is a short wavelength enhancement. The spectroscopic OCT image is consistent with the fact that longer wavelengths penetrate deeper than shorter wavelengths. The shallower structures have a green hue while deeper structures have a red hue. Melanocytes appear bright red in the spectroscopic

[47] U. Morgner, W. Drexler, F.X. Kärtner, X.D. Li, C. Pitris, E.P. Ippen, and J.G. Fujimoto, "Spectroscopic Optical Coherence Tomography," *Opt. Lett*. 25: 111-13 (2000).

OCT image, indicating that they are strongly scattering and red-shift light. The pigmented layer below the cell layer appears red in the spectroscopic OCT image. A melanocyte that is difficult to identify in the conventional OCT image is visible in the upper middle of the spectroscopic image.

Subcellular imaging has been demonstrated in a living, nontransparent, organism with ultrahigh-resolution and spectroscopic OCT. These results suggest a feasibility for assessing neoplastic changes in humans. The observations of greatest clinical relevance were the ability to identify active cell division and assess nuclear-to-cytoplasmic ratios, two important markers of malignant transformation. A change in the backscattering intensity from nuclei was also noted as a function of time. This is postulated to represent a change in the concentration or packing of chromatin, which may be of diagnostic relevance. These novel advancements yield not only dramatic improvements in OCT resolution, but also spectroscopic imaging in order to obtain functional or biochemical properties of the investigated tissue. At the same time, contrast is enhanced in a manner somewhat analogous to staining in histopathology, furthering the application of OCT for performing optical biopsies of biological tissue.

Imaging Devices for Optical Coherence Tomography

The development of OCT imaging devices is important for clinical applications. OCT has the advantage that it is fiber optically based and can readily be integrated with a wide range of existing clinical imaging instruments including microscopes, laparoscopes, endoscopes, and catheters. Several imaging devices have been designed and developed and evaluated in both animal and preliminary clinical studies.

The success of optical coherence tomography in clinical applications will depend in large part on the design and availability of delivery mechanisms that allow seamless integration with existing diagnostic imaging modalities. As an imaging technique capable of imaging human tissue at high resolution, OCT could lead to detection of pathology at earlier stages than currently possible, leading to improved patient prognosis. Several imaging devices have been designed and developed to investigate the feasibility of OCT for the clinical assessment of pathology of a variety of non-transparent tissue *in vivo*.

Colposcope

We have developed an OCT integrated colposcope that permits a simultaneous real time *en face* view of cervical pathology and OCT imaging. The system is based on a standard Zeiss colposcope. A custom attachment was designed and constructed to connect to the accessory port of the colposcope, permitting integration of OCT optics into a standard colposcopic examination. Two orthogonal scanning galvanometers are calibrated to allow scanning at an arbitrary position and orientation in a 4×4 cm area. The precision and noise of the driving waveforms are kept well below the resolution of the system to minimize the effect of jitter even at the large working distance of the colposcope. A visible 532 nm aiming beam at 250 μW was used to allow the operator to direct the OCT scan in the high magnification and intense white light illuminated field of the colposcope. The focal spot size of the system is ~30 μm and the axial resolution is ~15 μm. The OCT colposcope has been used in the clinical setting to successfully enable the acquisition of cross-sectional tomographic images of cervical tissue. OCT has demonstrated the ability to clearly delineate the epithelial and subepithelial structure of both normal and abnormal cervical tissue.[48] These studies were performed in collaboration with Dr. Annekathryn Goodman from the Massachusetts General Hospital.

[48] C. Pitris, X. D. Li, W. Drexler, J. G. Fujimoto, A. Goodman, M. E. Brezinski, "In Vivo Cervical Imaging with an Integrated Optical Coherence Tomography Colposcope," *Optics Letters* (in press).

Catheters and Endoscope probes

We have also developed single-mode fiber optic catheters and endoscopes capable of imaging the lumen of internal human organ systems. There are two general types of catheter/endoscope imaging devices that can image either radially in a transverse plane or longitudinally in a plane containing the axis of the catheter/endoscope.

We have developed and demonstrated a rotational scanning fiber-optic catheter. The body of the catheter consists of a flexible, hollow inner sleeve that fits loosely inside a stationary outer sheath. The flexible outer sheath allows the inner sleeve to slide freely while providing a smooth surface for the catheter to bend and pass through internal organ systems. The optical fiber is fixed to the center of the inner sleeve. A graded-index (GRIN) lens is attached to the distal end of the fiber, and a microprism is mounted on the distal end of the GRIN lens to direct the beam perpendicular to the fiber axis. The microprism, the GRIN lens, the inner sleeve, and the fiber are all attached to form a single unit that is scanned. The catheter operates by radially scanning the fiber and beam focusing optics to scan a cross sectional image through a hollow lumen. These catheters require the rotational scanning and coupling of a single mode optical fiber. Using these devices we have performed clinical imaging studies of the human gastrointestinal tract.[49] OCT endoscopy requires the use of flexible, narrow diameter probes that can be passed through the 2.8 mm diameter accessory port of a standard endoscope. We have developed catheters with diameters of 3.2 French or ~ 1 mm. Because of their small sizes these catheters can also be used to image the morphology of atherosclerotic lesions.[50] OCT has the capability of imaging plaque morphology with higher resolution than intravascular ultrasound.

A second catheter design has been developed which uses a linear scanning mechanism that avoids the complexity of coupling light into a fiber core across a rotating junction. In this design the fiber and beam steering optics are actuated in a push-pull manner along the axis of the transparent catheter housing. This generates an image in a longitudinal plane. The longitudinal scanning device has the advantage of producing an image that has a constant pixel density. In contrast, a radially scanning device has a decreasing pixel density as a function of the radial distance. We are currently evaluating different device designs that are optimized for specific clinical applications.

2.2 Optical Biopsy Using Optical Coherence Tomography

Arterial Imaging

Intracoronary stents have revolutionized the treatment of arterial occlusive disease. Stent implantation is now performed in over 700,000 coronary procedures annually.[52] It has improved the immediate safety and predictability of coronary angioplasty, and remains the only currently available approach to reduce both clinical and angiographic restenosis. Despite these benefits, stent implantation creates a unique and difficult to manage problem, in-stent restenosis, which occurs at a rate of more than 35%. Studies have suggested that the risk of developing in-stent restenosis be closely related to the adequacy of stent deployment. The criteria of adequate stent implantation include: (1) symmetric deployment of the stent; (2) adequate stent expansion such that all stent struts are pressed right up against the vessel wall (but without excessive pressure

[49] B.E. Bouma and G.J. Tearney, "Power-Efficient Nonreciprocal Interferometer and Linear-Scanning Fiber-Optic Catheter for Optical Coherence Tomography," *Opt. Lett.* 24(8): 531-33 (1996).

[50] J.G. Fujimoto, S.A. Boppart, G.J. Tearney, B.E. Bouma, C. Pitris, and M.E. Brezinski, "High Resolution *In Vivo* Intra-Arterial Imaging with Optical Coherence Tomography," *Heart* 82**,** 128-33 (1999)

[52] C.R. Narins and S.G. Ellis, "Prevention of In-Stent Restenosis," *Seminars in Interventional Cardiology* 3: 91-103 (1998).

against the wall); and (3) no presence of a stent border injury pattern such as residual dissection proximal or distal to the stent.[53,54]

Intravascular Ultrasound (IVUS) has been used for quantitatively monitoring and guiding stent deployment. Compared to quantitative angiography, IVUS provides better resolution in determining the stent and the vessel cross sectional dimensions. It has been shown that, within the resolution limit of IVUS (~75 μm), a better accuracy in determining those dimensions could lead to the relative reduction of in-stent restenosis by about 38%.[52] However the absolute rate of in-stent restenosis is still very high (>20%) even with IVUS guidance for stent deployment. More accurate determination of the stent and vessel cross sectional dimensions could potentially result in a further decrease of the in-stent restenosis rate and consequently improve patient outcome. Thus a need exists for imaging the stent and guiding its deployment with higher resolution. In addition it is questionable whether it is cost effective to perform the IVUS examination.

OCT is capable of tissue cross sectional imaging with resolution of 1-15 μm and represents a improvement of 10 to 50 times over the currently available IVUS. Technology advances permit real time, *in vivo* OCT imaging.[55] The fiber optically based OCT catheter is flexible and compact, and it could be potentially made very inexpensive compared to the IVUS catheter. High-speed catheter-based OCT has been developed for *in vivo* intravascular imaging in rabbits.[50] Microstructure was sharply defined within the aorta wall.

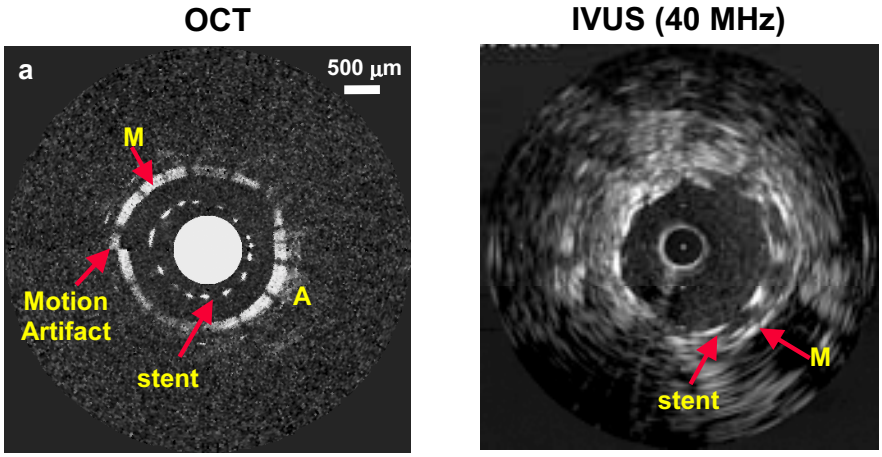

Figure 16: Real time in vivo OCT image of a rabbit abdominal aorta within which a stent has been deployed (a); and the corresponding 40 MHz IVUS image (b). A: Adventitia. M: Media.

A portable, high-speed OCT system has recently been used for *in vivo* monitoring and guiding stent placement in the abdominal aorta of a normal New Zealand White rabbit. A compact SLD was used as a low coherence light source which gives ~10 μm axial resolution. Both OCT and IVUS images were acquired from the aorta after the stent was deployed. A state-of-the-art 40 MHz IVUS catheter was used, representing the highest IVUS resolution clinically available. As shown in Figure 16, the media and the adventitia within the aorta wall were clearly delineated on OCT images as compared to IVUS images. In addition, high contrast was noted between the vessel wall and the stent struts. The separation between the stent strut and the vessel wall and

[53] A. Oshima, D. Itchhaporia, and P. Fitzgerald, "New Developments in Intravascular Ultrasound," *Vascular Medicine* 3: 281-90 (1998).

[54] Y. Yoshitomi, S. Kojima, M. Yano, T. Sugi, Y. Matsumoto, and M. Kuramochi, "Benefit of Iintravascular Ultrasound in Wiktor Stent Implantation," *Catheterization & Cardiovascular Interventions* 47: 28-35 (1999).

[55] G.J. Tearney, M.E. Brezinski, B.E. Bouma, S.A. Boppart, C. Pitris, J.F. Southern, and J.G. Fujimoto, "*In Vivo* Endoscopic Optical Biopsy with Optical Coherence Tomography," *Science* 276: 2037-39 (1997).

the stent positional symmetry with respect to the vessel, two important parameters in evaluating the adequacy of stent placement, can be clearly identified within the resolution limits of OCT. During OCT imaging, low pressure and small volume saline injection was required in order to compensate the signal attenuation due to strong scattering predominantly by red blood cells. Saline injection was also used for IVUS imaging in order to compare OCT with IVUS images under the same conditions. Superior methods are becoming available to deal with the blood scattering by using index matching instead of saline injection, which would be more practical for *in vivo* patient imaging. This work strongly suggests a role for OCT in guiding and monitoring stent deployment since OCT provides superior resolution and contrast over IVUS. Future investigation will focus on *in vivo* examination of an aorta with vulnerable plaques in rabbits. These studies are being performed in collaboration with Dr. Hermann Gold from the Massachusetts General Hospital.

Orthopedics

Osteoarthritis (OA) is the most common cause of disability in the United States, symptomatically affecting about 14% of the adult population. The earliest pathological changes start with articular cartilage degeneration, including cartilage loss (thinning effect), fibrillation and surface erosion.[56] It has been suggested by recent research that osteoarthritic progression can be arrested or modified through surgical and/or pharmacological intervention if the articular degeneration can be identified at an early stage.[57] Since the cartilage surface is only a few millimeters in thickness, a diagnostic imaging technique capable of high-resolution imaging of articular cartilage *in vivo* would be invaluable to detect disease, follow its progression and monitor therapeutic effectiveness and outcome. The resolutions of current imaging modalities such as plain X-ray radiography, computerized tomography, MRI and ultrasound range from ~1 mm to ~100 μm, which is not sufficient for diagnosing early cartilage degeneration. Although arthroscopy is widely used in diagnosis of joint disorders, it provides only magnified views of the articular surface. OCT could potentially overcome the limitations of the current rheumatologic imaging modalities. It is an attractive imaging alternative for osteoarthritis because it permits imaging of tissue microstructures *in situ* and real time with unprecedented high resolution (2-10 μm). It also provides unique optical contrast such as polarization sensitive birefringence and spectroscopic signature that could be used to obtain clinically useful physiological and/or biochemical information.[58,47] OCT is attractive for articular imaging also because it is compact and portable, well suited for an outpatient setting and the tight confines of an operation room.

OCT imaging is performed with a portable real time OCT system using a hand-held forward imaging probe. In collaboration with investigators at West Roxbury VA Hospital and Brigham and Women's Hospital, preliminary results obtained during open knee surgeries demonstrate that cartilage degeneration can be assessed with OCT. In particular, polarization sensitivity assessed by OCT (as indicated by the pronounced layered contours on the OCT images in Figure 17) in adjunct to microstructural information offers a unique, clinically useful biochemical indicator of cartilage degeneration. The loss of polarization sensitivity indicates the loss of collagen fiber organization, which is an early indicator of osteoarthritis.

---

[56] M.E. Adams and C.J. Wallace, "Quantitative Imaging of Osteoarthritis," *Seminars in Arthritis & Rheumatism* 20(6 Suppl 2): 26-39 (1991).

[57] P. Needleman and P.T. Manning, "Interactions Between the Inducible Cyclooxygenase (COX-2) and Nitric Oxide Synthase (iNOS) Pathways: Implications for Therapeutic Intervention in Osteoarthritis," *Osteoarthritis & Cartilage* 7 (4): 367-70 (1999).

[58] J.F. de Boer, T.E. Milner, M.J.C. van Gemert, and J.S. Nelson, "Two-Dimensional Birefringence Imaging in Biological Tssue by Polarization-Sensitive Optical Coherence Tomography," *Opt. Lett.* 22(12): 934-36 (1997).

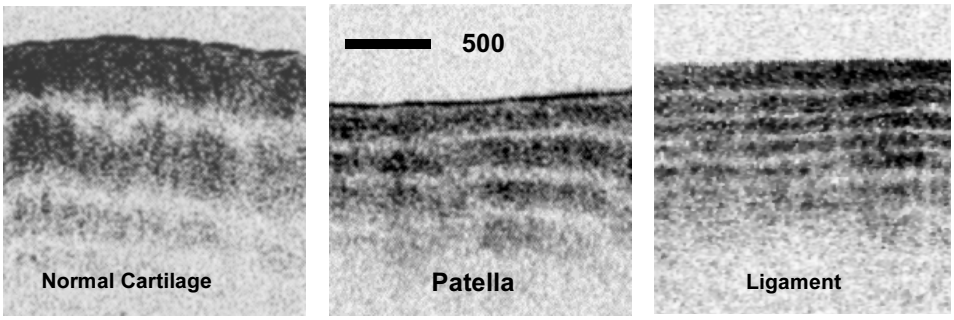

Figure 17: Polarization sensitivity of different birefringent tissues assessed by a portable, single detector OCT system in real time. (a) Normal articular cartilage; (b) Patella cartilage; (c) Anterior Cruciate Ligament. The birefringence Δn increases from (a) to (c). The calculated birefringence Δn's for (a) to (c) are $\times 10^{-3}$, $\times 10^{-3}$, $\times 10^{-3}$, respectively.

Recent studies focus on quantitative assessment of collagen fiber organization in terms of birefringence, $\Delta n = n_x - n_y$, which is the difference in indices of refraction along the fast and slow axes. Δn could potentially be used to quantitatively characterize cartilage degeneration. The birefringence has been traditionally characterized using a bench-top, free space OCT system with polarized low coherence light.[58] We have demonstrated that, with a single detector portable OCT system and fiber delivered unpolarized low coherence light, birefringence can also be quantified. It can be shown that the periodicity of the layered contours is inversely related to Δn. We have demonstrated that our portable real time OCT system can be readily used for characterizing birefringence for different tissues. As shown in Figure 18, Δn's assessed by OCT for tissues with different degrees of fiber organization and density are in the correct trend, and the results are of the same order as those from other biological tissues.[58]

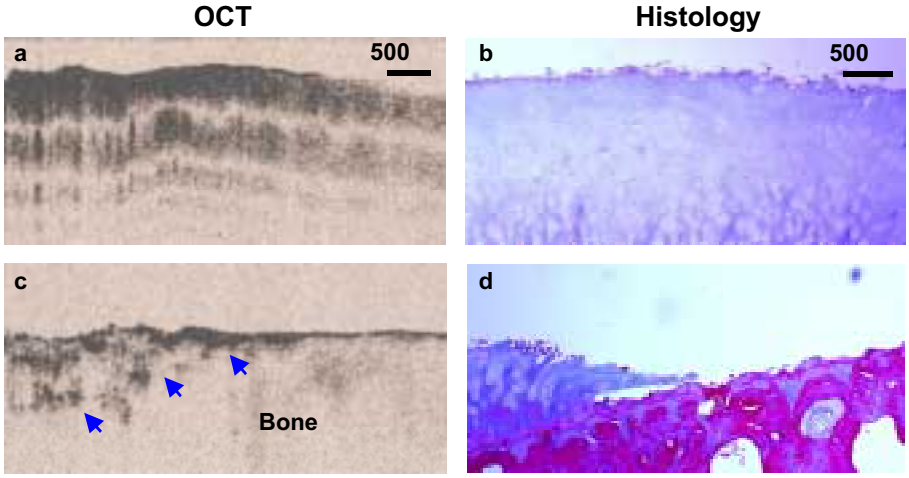

Figure 18: Real time *in vivo* OCT images of human joint cartilage and histologies; (a) demonstrates an OCT image of normal articular cartilage and (b) is the corresponding histology with trichrome blue staining. The cartilage is thick and the pronounced birefringence implies collagen fiber is in an organized state (normal). (c) illustrates an OCT image of osteoarthritic cartilage and (d) is the corresponding histology. The bone and cartilage interface, indicated by arrows, can be clearly delineated on the OCT image as well as on corresponding histology. The loss of birefringence in (c) implies the loss of collagen fiber organization and therefore the cartilage is degenerated.

Following the preliminary studies, recent investigations also focus on co-registration of OCT images with histopathology. After the knee joint is fully exposed during the knee replacement surgery, regions of interest on the articular surfaces are identified. Two dots are marked at the boundary of the region of interest with Methelyne blue and a third dot is also marked as an orientation identifier. With the help of a visible aiming beam, the surgeon aligns the scanning OCT beam between the marked two dots. OCT images are saved in a computer in digital format and recorded to a super VHS for off line analysis. After OCT imaging, special cutting blocks are used for removing the joint to ensure regions of interest are intact. The removed specimens are immediately fixed in 10% Formalin and sent to a histopathology lab for processing with Trichrome blue staining. Preliminary results show that real time *in vivo* OCT images correlate well with histopathology for normal and pathologic cartilage (Figure 18). The transitional zone of the degenerated cartilage indicated by onset of loss of polarization sensitivity on the OCT image, also correlates with histopathology.

OCT images are taken at 4 frames per second. Each frame has 256 x 512 pixels corresponding to a 3 x 5 mm^2 tissue cross section. Future work will focus on increasing the frame rate to further minimize motion artifact. Pixel density also needs to be increased to reduce sampling error and fully utilize the superb resolution provided by the OCT light source. Different staining schemes will be considered for histopathology processing of the specimens in order to correlate polarization sensitivity assessed by OCT to the birefringence of the cartilage. Although OCT images are taken during open knee surgeries, this study has demonstrated the feasibility of using OCT in assessing osteoarthritis with micron scale resolution. Small OCT catheters might be combined with the micro-arthroscope to offer an opportunity for diagnosing articular cartilage degeneration with micron scale resolution. These studies are being performed in collaboration with Dr. Scott Martin from the West Roxbury Veterans Administration Hospital and the Harvard Medical School.

Early Neoplastic Diagnosis

Female Reproductive System

The dysplastic human cervix is an excellent model system that can be used to systematically investigate and quantitatively evaluate OCT *in vivo*. Although the incidence of cervical neoplasia is very common, there are only 13,700 new cervical cancer cases per year resulting in 4,900 deaths in the United States.[59] Early identification of cervical neoplasia improves patients' prognosis; the screening technique of choice, the Papanikolaou Smear, despite its accuracy shortcomings, has significantly contributed to the reduction of deaths associated with cervical cancer. Neoplasias are most responsive to medical intervention at early stages, prior to undergoing metastasis. When these disorders arise from known premalignant states, and if a detection method exists, high risk populations can be screened to reduce patient morbidity and mortality.

The diagnosis of neoplasia and early cancer is based on colposcopy and biopsy, i.e. the visual examination of the surface of the cervix under high magnification and white light illumination and the simultaneous acquisition of biopsies. Dysplastic changes of the cervical epithelial layer have been extensively examined and the progression of dysplasia to cancer has been carefully mapped both histologically and colposcopically.[60,61] Changes associated with neoplasia include cellular and microstructural alterations. The well defined pathology, progression, and endpoints, along with ease of accessibility and frequency of colposcopic procedures, make the cervix a good

[59] S.H. Landis, T. Murray, S. Bolden, and P.A. Wingo, "Cancer Statistics," *CA Cancer J. Clin*. 49: 8-31 (1999).

[60] R.J. Kurman, P.F. Kaminski, and H.J. Norris, "The Behavior of Endometrial Hyperplasia. A Long-Term Study of "Untreated" Hyperplasia in 170 Patients," *Cancer* 56: 403-12 (1985).

[61] M.C. Anderson, J.A. Jordan, A.R. Morse, and F. Sharpl, Integrated Colposcopy. New York: Chapman and Hall Medical, 1996.

model system for the evaluation of the diagnostic capabilities of OCT. It is unlikely that OCT imaging will have a direct clinical application for cervical cancer detection. However, OCT imaging studies in the cervix can provide insight into the relationship of OCT images to the architectural and cellular morphology of tissues as well as the mechanisms of contrast in OCT images and tissue optical properties. Conclusions can be drawn which are generalizable to other epithelial cancers.

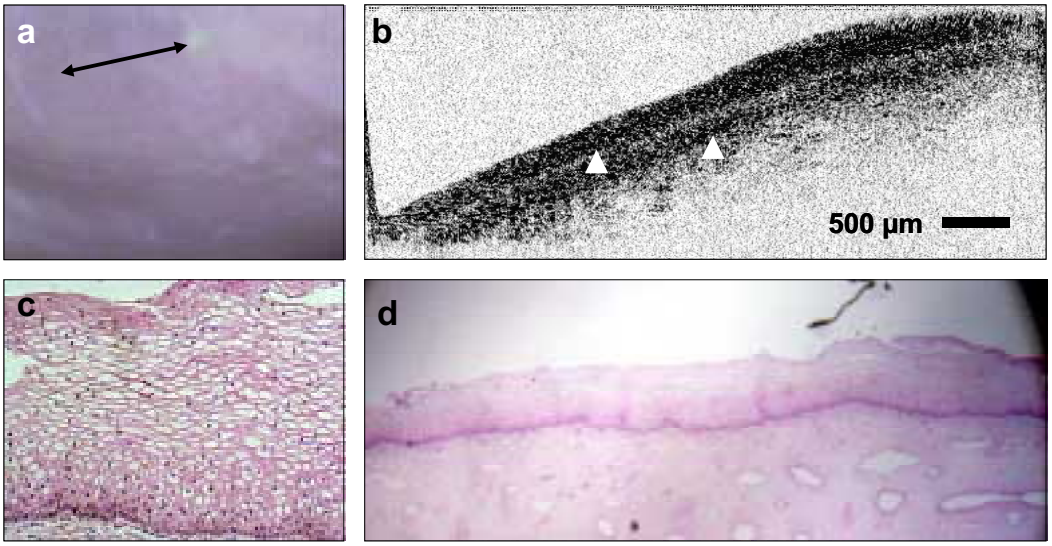

Figure 19: Normal human cervix imaged *in vivo*. (a) Photograph of the cervix as viewed through the colposcope. The extent of the OCT scanning is marked by the arrow. (b) OCT image of the same area. c&d. Histologic cross-sections of the cervical tissue at 100x and 12.5x. The arrows in the OCT image mark the uniform and layered appearance characteristic of normal cervical epithelium. (Size: 2.5 x 5 mm, Resolution: 15 x 22 µm)

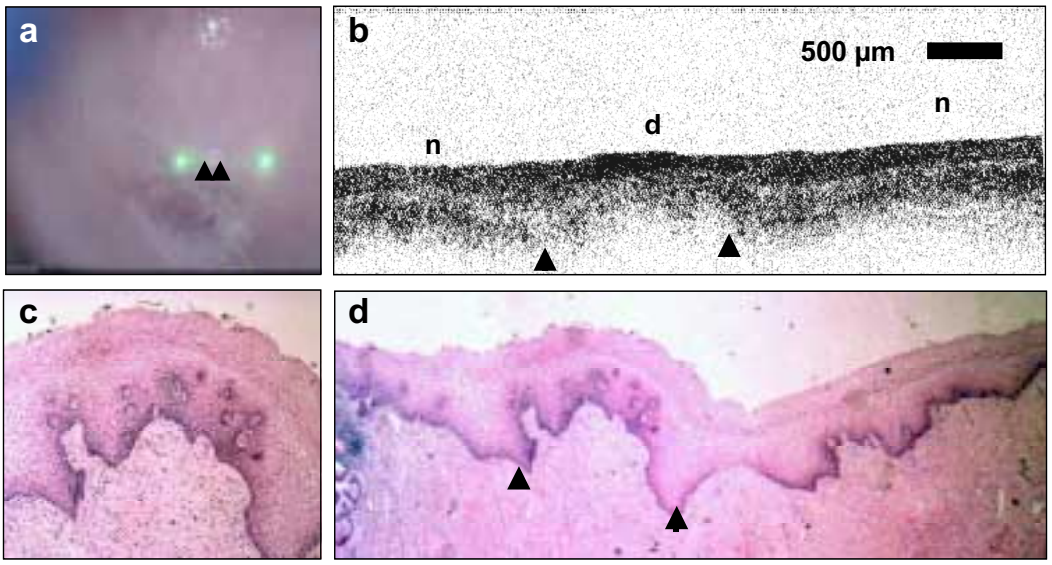

Figure 20: Dysplastic human cervix imaged *in vivo*. (a) Photograph of the cervix as viewed through the colposcope. The extent of the OCT scanning is marked by the guiding beam spots. (b) OCT image of the same area. (c, d) Histologic cross-sections of the cervical tissue at 100x and 12.5x. The arrows in the colposcopic image, OCT image and histology indicate the margins

of a focal dysplastic area. Normal epithelium (n) and a focal area of dysplasia (d) are visible in the OCT image. (Size: 2.5 x 5 mm, Resolution: 15 x 22 µm).

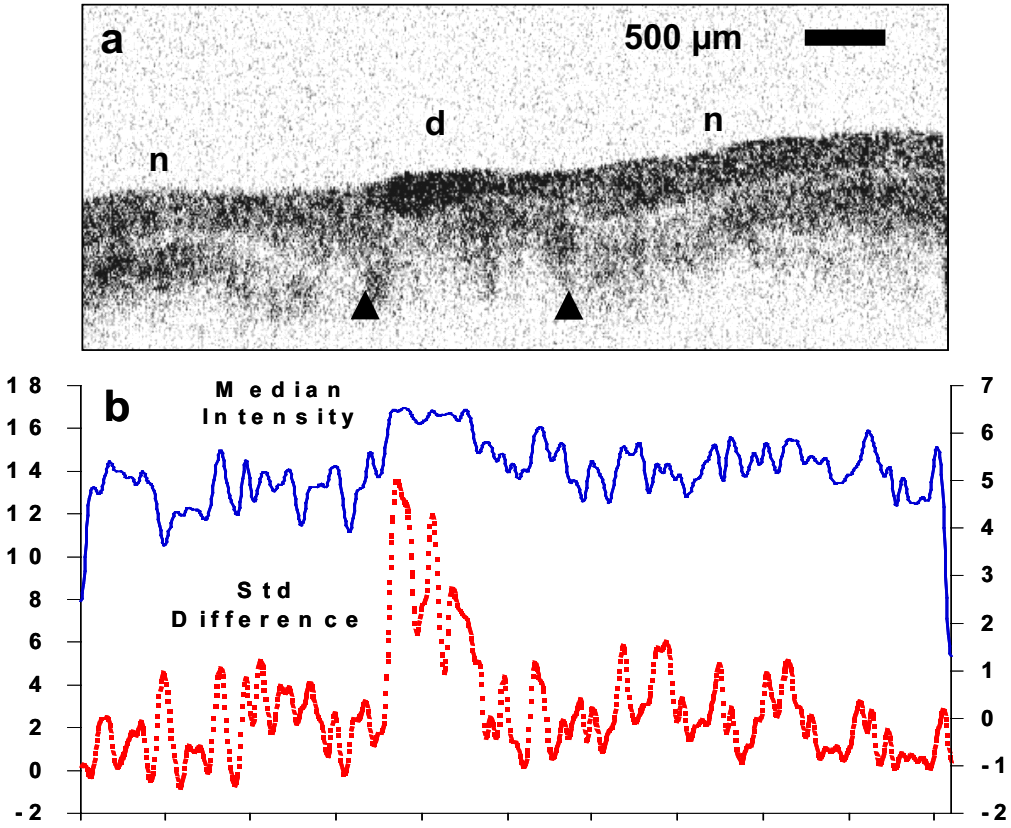

Figure 21: (a) The segmented OCT image of Figure 20 (b). The epithelium is divided into two regions, Superficial and Intermediate/Parabasal/Basal, for measurement purposes. (b) Graph of the median intensity of the top region of the epithelium (solid blue line) and the differences of standard variance of the intensity (dash red line) between the two layers.

We have recently begun preliminary OCT imaging studies of cervical cancer with a prototype OCT colposcope. This design enables *en face* viewing of pathology on the surface of the cervix, while simultaneously controlling the scan pattern of the OCT image. Ten patients have been imaged to date. Figure 19 shows an example of an OCT image of a normal cervix, a coloposcopic view of the area scanned, and corresponding histology. Figure 20 shows an example of a focal mild dysplasia, with a corresponding colposcopic view and histology. One powerful advantage of OCT imaging is that since image information is available in electronic form, image processing algorithms can be applied to extract features which could be relevant to clinical diagnosis. Figure 21 shows a very preliminary result which applied image processing to *in vivo* cervical OCT images in an attempt to extract the thickness of different epithelial structures. This data is very preliminary, so no conclusions can be drawn at this time. The advantage of image processing approaches is that they can be applied to large amounts of image data in order to rapidly extract clinically important information. These studies are being performed in collaboration with Dr. Annekathryn Goodman from the Massachusetts General Hospital.

Gastrointestinal Tract

Barrett's esophagus represents a clinical situation where conventional excisional biopsy can have unacceptable false negative rates due to sampling errors. Carcinoma of the esophagus is one of

the most lethal of all cancers with a 5-year survival rate <10%. In 1999, 12,500 new cancers and 12,200 deaths are expected in the USA alone.[59] Barrett's esophagus has been identified as the single most important risk factor for developing adenocarcinoma. Barrett's esophagus is a premalignant condition where normal squamous epithelium is replaced with metaplastic columnar epithelium. Metaplastic columnar epithelium develops in about 10% of patients with chronic gastroesophageal reflux disease.[62] Data on the risk of progression to adenocarcinoma in Barrett's esophagus vary widely with a median of about 1/100 patient years, indicating a 30 to 125 times increased risk.[63,64] Early identification of esophageal cancer, before symptoms manifest, improves the survival rate dramatically. Therefore, endoscopic surveillance of patients suffering from Barrett's esophagus every 6-18 months is recommended. Endoscopic screening currently involves random biopsies every 2 cm. However, because high grade dysplasia is usually not visible endoscopically, excisional biopsy may miss areas of high grade dysplasia or small foci of carcinoma.[65] OCT can provide real time image information on tissue pathology and could be used to guide conventional excisional biopsy to reduce sampling errors. This would provide a low cost screening technique for Barrett's esophagus in patients with gastroesophageal reflux disease (GERD).

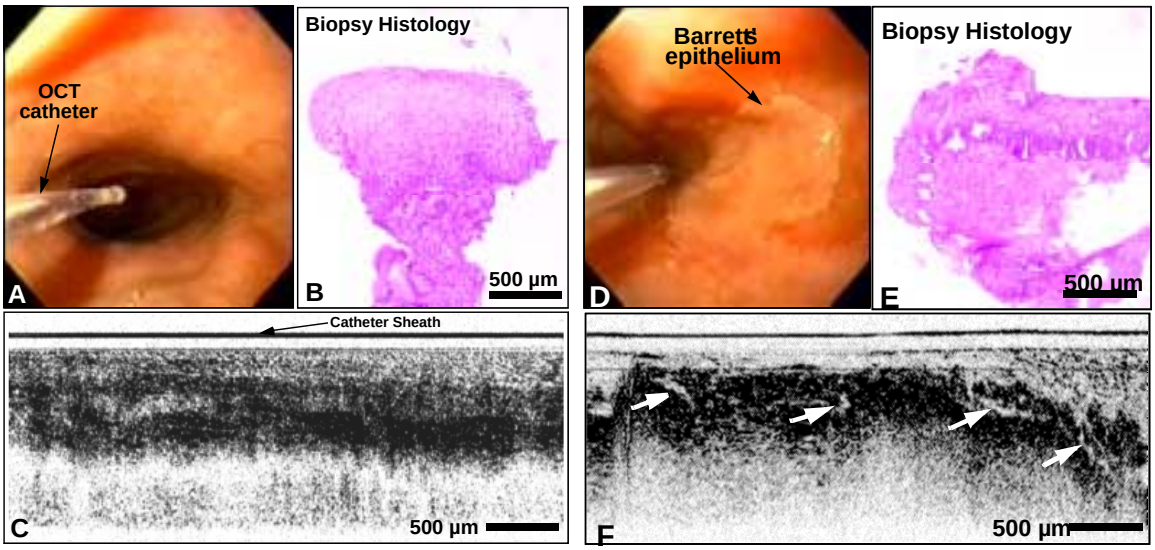

Figure 22: Endoscopic OCT images of the human esophagus showing normal and Barrett's metaplasia. The figures show endoscopic view (A,D), OCT images taken with a longitudinal scanning imaging catheter (B,E)), and corresponding histology from punch biopsies (C,F) of normal and Barrett's metaplasia. Barrett's metaplasia is a precursor to carcinoma of the esophagus.

We have investigated the feasibility of using OCT for imaging the esophagus via a compact OCT imaging catheter. Previous *in vitro* imaging studies using standard 10-15 µm resolution OCT in

---

62 J. Winters et al., "Barrett's Esophagus. A Prevalent, Occult Complication of Gastroesophageal Reflux Disease," *Gastroenterology* 92: 118-24 (1987).

63 A.J. Cameron, B.J. Ott, and W.S. Payne, "Low Iincidence of Adenocarcnoma in Columar Lined (Barrett's) Esophagus," *New England Journal of Medicine* 313: 857-59 (1985).

64 S.J. Spechler, A.H. Robbins, H.B. Rubins, M.E. Vincent, T. Heeren, W.G. Doos, T. Colton, and E.M. Schimmel, "Adenocarcinoma and Barrett's Esophagus. An Overrated Risk?," *Gastroenterology* 87, 927-33 (1984).

65 A.T. Axon, "Cancer Surveillance in Ulcerative Colitis-- a Time for Reappraisal," *Gut* 35: 587-89 (1994).

comparison to histopathology have been performed on normal as well as abnormal human GI pathologies, including Barrett's esophagus, squamous carcinoma, and adenocarcinoma of the colon. Standard resolution OCT can clearly distinguish the squamous epithelium of the normal esophagus from glandular structure present in Barrett's esophagus. In contrast to the uniform, highly backscattering layer of normal squamous epithelium Barrett's esophagus appears as a highly non-uniform and disorganized structure. The lamina propria and muscularis mucosa layers, as well as blood vessels and lymphoid aggregates, are also identified. In addition, *in vitro* images of human tissue have shown the capability of OCT to clearly differentiate between columnar and squamous epithelium. Real time, *in vivo* catheter/endoscope based OCT imaging of the upper GI tract has also been demonstrated. The esophagus was imaged *in vivo* from the pharynx to the lower esophageal sphincter by using a transverse scanning catheter. *In vivo* OCT images of the esophagus (Figure 22) allowed visualization of the layered structure of the esophageal wall. These experiments suggest that OCT has the potential to be an effective screening technology for Barrett's esophagus. These studies are being performed in collaboration with Dr. Jacques Van Dam from the Brigham and Women's Hospital and Drs. Hiroshi Mashimo and Muthoka Mutinga from the West Roxbury Veteran's Administration Medical Center.

Publications List

Pitris, C, A. Goodman, S.A. Boppart, J.J. Libus, J.G. Fujimoto, and M.E. Brezinski. "High Resolution Imaging of Gynecological Neoplasms using Optical Coherence Tomography," *Obstetrics and Gynocology* 93: 135-39 (1999).

Herrmann, J., C. Pitris, B.E. Bouma, S.A. Boppart, J.G. Fujimoto, and M.E. Brezinski, "High Resolution Imaging of Normal and Osteoartheritic Cartilage with Optical Coherence Tomography," *J. Rheumatology* 26(3): 627-35 (1999).

Boppart, S.A., J. Herrmann, C. Pitris, D.L. Stamper, M.E. Brezinski, and J.G. Fujimoto, "High-Resolution Optical Coherence Tomography Guided Laser Ablation of Surgical Tissue," *J. Surgical Research* 82: 275-84 (1999).

Fujimoto, J.G., S.A. Boppart, G.J. Tearney, B.E. Bouma, C. Pitris, and M.E. Brezinski, "High Resolution In Vivo Intra-Arterial Imaging with Optical Coherence Tomography," *Heart* 82: 128-33 (1999).

Brezinski, M.E., and J. G. Fujimoto, "Optical Coherence Tomography: High Resolution Imaging in Nontransparent Tissue," *IEEE J. Selected Topics in Quantum Electron.* 5: 1185-92, (1999).

Drexler, W., U. Morgner, F.X. Kärtner, C. Pitris, S.A. Boppart, X.D. Li, E.P. Ippen, J.G. Fujimoto, "In Vivo Ultrahigh Resolution Optical Coherence Tomography," *Opt. Lett.* 24: 1221-23 (1999).

Boppart, S.A., A. Goodman, J. Libus, C. Pitris, C. Jesser, M.E. Brezinski, and J.G. Fujimoto, "High Resolution Imaging of Endometriosis and Ovarian Carcinoma with Optical Coherence Tomography: Feasibility for Laparoscopic-Based Imaging," *Brit. J. Obstetrics Gynecology* 106: 1071-7 (1999).

DiCarlo, C.D., W.P. Roach, D.A. Gagliano, S.A. Boppart, D.X. Hammer, A.B. Cox, and J.G. Fujimoto, "Comparison of Optical Coherence Tomography (OCT) Imaging of Cataracts with Histopathlogy," *J. Biomedical Opt.* 4: 450-58 (1999).

Jesser, C.A., C. Pitris, D.L. Stamper, S.A. Boppart, G.P. Nielsen, M.E. Brezinski, and J.G. Fujimoto, "High Resolution Endoscopic Evaluation of Transitional Cell Carcinoma with Optical Coherence Tomography," *Brit. J. Radiology* 72: 1170-76 (1999).

Morgner, U., W. Drexler, F.X. Kärtner, X.D. Li, C. Pitris, E.P. Ippen, and J.G. Fujimoto, "Spectroscopic Optical Coherence Tomography," *Opt. Lett.* 25: 111-13 (2000).

Pitris, C., C.A. Jesser, S.A. Boppart, D. Stamper, M.E. Brezinski, and J.G. Fujimoto, “Feasibility of Optical Coherence Tomography for High Resolution Imaging of Human Gastrointestinal Tract Malignancies,” *J. Gastroenterology* 35: 87-92 (2000).

Fujimoto, J.G., C. Pitris, S.A. Boppart, and M.E. Brezinski, "Optical Coherence Tomography, An Emerging Technology for Biomedical Imaging and Optical Biopsy," *Neoplasia* 2: 9-25 (2000).